Density-functional study of oxygen vacancies in monoclinic tungsten oxide

2006 J. Phys.: Condens. Matter 18 7361

(http://iopscience.iop.org/0953-8984/18/31/028)

INSTITUTE OF PHYSICS PUBLISHING JOURNAL OF PHYSICS: CONDENSED MATTER

J. Phys.: Condens. Matter **18** (2006) 7361–7371 doi:10.1088/0953-8984/18/31/028

Density-functional study of oxygen vacancies in monoclinic tungsten oxide

C Lambert-Mauriat and V Oison

Université Paul Cézanne Aix–Marseille III, Laboratoire Matériaux et Microélectronique de Provence, UMR-CNRS 6137, Faculté des Sciences et Techniques, Case 152, Campus St Jérôme Avenue Escadrille Normandie–Niemen, 13397 Marseille Cedex 20, France

E-mail: lambert@L2MP.fr and vincent.oison@L2MP.fr

Received 7 February 2006, in final form 22 June 2006
Published 21 July 2006
Online at stacks.iop.org/JPhysCM/18/7361

Abstract

A detailed study of the formation of neutral oxygen vacancies in monoclinic tungsten oxide (WO_3) is performed within the framework of the self-consistent first-principles SIESTA method. This work reveals that the neutral oxygen vacancies are anisotropic with a strong correlation to the structural anisotropy of the WO_3 monoclinic room temperature phase. We show that most of the structural relaxation around the vacancies occurs along a single straight line of W–O–W bonds and that the lowest energy corresponds to the formation of vacancies along the [001] crystallographic direction, where long and short W–O bonds alternate. Moreover, vacancies lead to the partial filling of the conduction band, in which 5d electronic states of the neighbouring W atoms dominate. In term of Mulliken population, the initial charge carried by the removed oxygen atom is almost recovered on the O and W atoms closest to the vacancy.

(Some figures in this article are in colour only in the electronic version)

1. Introduction

Tungsten oxide (WO_3) is slightly oxygen deficient, which makes it an interesting n-type semiconductor material for technological applications. Hence, the physical and chemical properties of WO_3 have been experimentally studied for a long time, in particular its phase diagram, which presents numerous polymorph transformations between 230 and 1015 K [1]. The electrochromic properties of WO_3 were first investigated [2–5]. The possibility of ion intercalation/deintercalation has given rise to several potential applications in devices such as cathodes for rechargeable batteries [6] or electrodes for water photo-electrolysis [7]. More recently WO_3 has been investigated as a sensitive layer for gas sensor applications, in order to detect small quantities of NO_x [8–14], NH_3 [15, 16] or ozone [17–19]. These devices operate by measuring the variation of the resistivity of the sensitive layer under different atmospheres.

0953-8984/06/317361+11$30.00

In such applications surface oxygen vacancies play a major role in electrical conductivity [20] as well as in gas detection [21]. Nevertheless, the electronic transfer between adsorbed species and the WO_3 film is still not well understood.

At room temperature, the crystallographic phase of WO_3 is monoclinic (space group $P2_1/n$). This monoclinic room temperature (Mono RT) structure contains eight WO_3 per unit cell, each W atom being six-fold coordinated by oxygen atoms. Thus, the study of oxygen vacancy formation in this phase requires calculations on large supercells made of several W_8O_{24} unit cells. Because of the size of this system, the first theoretical works on the electronic structure of WO_3 concerned the simple cubic phase and its bronzes [22, 23]. More recently, different studies have dealt with the bulk properties of the various WO_3 [24, 25] crystallographic phases, but the theoretical studies of defects are limited to the effects of oxygen vacancy formation on the electronic structure of amorphous WO_3 [26] and on the theoretical cubic phase [27]. Most of these theoretical investigations are performed by means of standard plane-wave density functional calculations. Although precise, these approaches are limited by the size of the system studied. As plane-wave density functional calculations become too time-consuming, SIESTA implementation [28, 29] is increasingly used as an alternative to study such large systems. This code uses a reduced and flexible basis set of numerical atomic orbitals and optimizes the resolution of the electronic structure. Hence, in comparison with standard plane-wave density functional calculations, a gain in calculation time higher than one order of magnitude is achieved in many cases.

In this paper, we present a detailed analysis of the formation of oxygen vacancies in the bulk Mono RT. A self-consistent first-principles SIESTA method carrying out geometry optimizations is used. Moreover, the local-density approximation (LDA) gives the lattice constants of WO_3 [24] in better agreement with experiment than the generalized gradient approximation (GGA), and the GGA functionals improve cohesive energies [30–32]. Therefore these two exchange–correlation functionals are systematically used. Due to the structural anisotropy of the Mono RT phase, three non-equivalent oxygen vacancies are considered in this work.

This paper is organized as follows. Section 2 is devoted to the computational details. The optimized basis set used in the present SIESTA simulations is validated on the bulk properties of the phase diagram of WO_3: results are compared to experiments and previous calculations [24, 25]. The results show that the properties of a vacancy strongly depend on the orientation of the broken W–O bonds. Finally, the main results of this study are summarized in section 4.

2. Computational details

Ab initio calculations are performed using the SIESTA implementation [28, 29] within the framework of the density-functional theory (DFT) [33]. The exchange–correlation potential is treated not only within the local-density approximation (LDA) but also within the generalized gradient approximation (GGA) using parameterization proposed by Perdew–Burke–Ernzerhof [34]. Core electrons are treated within the frozen core approximation in which norm-conserving Troullier–Martins [35] pseudopotentials, including nonlinear core corrections for W, are used.

The wavefunction of the valence electrons ($2s^2 2p^4$ for O and $6s^2 5d^4$ for W) is expanded on a localized basis set consisting of finite-range pseudo-atomic orbitals [36]. A double-ζ basis set is used for both atoms: each atomic valence state is described by two localized wavefunctions. In order to allow polarization, 3d and 6p orbitals are included for O and W species, respectively. Cutoff radii for the double-ζ basis set are optimized in order to reproduce as accurately as

Table 1. Lattice parameters of the Mono RT phase calculated within the LDA and the GGA. Comparison with previous calculations and experiments.

		a (Å)	b (Å)	c (Å)	β (deg)
LDA	SIESTA	**7.24**	**7.45**	**7.61**	**90.5**
	Reference [24]	7.37	7.46	7.64	90.6
	Reference [25]	7.30	7.49	7.32	90.1
GGA	SIESTA	**7.48**	**7.66**	**7.85**	**90.4**
	Reference [24]	7.55	7.62	7.83	90.2
Expt	Reference [41]	7.31	7.54	7.69	90.9

possible the experimental lattice parameters of each structure [37–41] in the phase diagram of WO_3. The geometrical optimization procedure consists in relaxing atomic positions and cell parameters with a maximum force tolerance of 0.02 eV Å^{-1} on each atom and a maximum stress tolerance of 1 GPa for each component of the stress tensor. In comparison with the previous SIESTA work [25], our optimization of basis sets leads to the use of quite large radii for orbitals localized on oxygen atoms: 5.3 and 5.2 Bohr for the atomic functions corresponding to the 2s orbitals, 5.9 and 2.7 Bohr for those corresponding to the 2p orbitals, and 2.6 Bohr for those corresponding to the 3d orbitals. In all the calculations, the **k**-point sampling is equivalent to an $8 \times 8 \times 8$ **k**-mesh grid in the cubic phase containing one WO_3 per unit cell.

The formation of neutral oxygen vacancies (V) is studied by means of the supercell technique. The vacancy formation consists in the following reaction:

$$W_nO_{3n} \longrightarrow W_nO_{3n-1}V + \tfrac{1}{2}O_2, \tag{1}$$

where n is the number of W atoms per supercell. At constant volume, the corresponding vacancy formation energy E_f is given by

$$E_f = E(W_nO_{3n-1}V) + \tfrac{1}{2}E(O_2) - E(W_nO_{3n}). \tag{2}$$

Herein, the oxygen molecule reference energy is the energy of the spin-triplet state.

Four supercell sizes are considered: (i) $n = 8$, corresponding to the Mono RT unit cell; (ii) $n = 16$, consisting in a doubling of the unit cell along the W–V–W direction; (iii) $n = 32$, which is built by quadrupling the unit cell along the W–V–W direction; and (iv) $n = 64$, obtained by doubling the three crystallographic axes. In all the calculations the removed O atom is replaced by a so-called ghost atom in order to keep the size of the basis set constant.

3. Neutral oxygen vacancy

3.1. Geometrical structure of the Mono RT phase

The experimental lattice parameters of the Mono RT structure, deduced from neutron diffraction data [38, 41], are given in table 1: the unit cell, which contains eight WO_3, can be generated from only the atomic positions of two non-equivalent WO_3. The W atoms are located at the centre of distorted octahedrons made of six O atoms. Each oxygen atom forms two W–O bonds. In this study, the three non-equivalent oxygen atoms, denoted O_a, O_b and O_c, are distinguished: the indices a, b and c indicate the direction of the W–O bond. In order to simplify the structural study, only the six W–O bonds in one of the two non-equivalent octahedrons are considered, those in the second octahedron being very similar. As shown in table 1, the lattice parameters obtained at the equilibrium volume from the present work are in good agreement with those reported in previous theoretical works [24, 25]. The relaxed structure obtained within the GGA is displayed in figure 1. Along the **a** direction, the oxygen atoms are almost

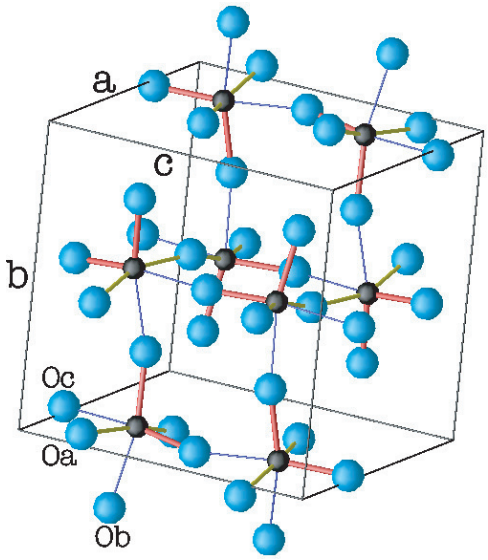

Figure 1. Relaxed GGA structure of the Mono RT unit cell of WO_3. W and O atoms are represented by small (black) and large (blue) spheres, respectively. Short W–O distances (∼1.8 Å) are represented by thick (red) segments, medium distances (∼1.9 Å) by medium (yellow) segments and long distances (∼2.1 Å) by thin (blue) segments.

Table 2. W–O bond lengths obtained in Mono RT WO_3 after relaxation of the atomic positions within the LDA and the GGA. Comparison with experiments.

		LDA	GGA	Expt [41]
$W\cdots O_a$ (Å)	Medium	1.935	1.940	1.931
	Medium	1.881	1.916	1.867
$W\cdots O_b$ (Å)	Short	1.815	1.819	1.782
	Long	2.027	2.102	2.092
$W\cdots O_c$ (Å)	Short	1.787	1.791	1.740
	Long	2.094	2.178	2.185

equidistant to a W atom, whereas along the **b** and **c** crystallographic directions long and short W–O bonds alternate. The calculated W–O bond lengths are reported in table 2. Their values are comprised between 1.79 and 2.09 Å in the LDA and between 1.79 and 2.18 Å in the GGA. In both cases, the W–O_a bond lengths are in good agreement with the experimental ones [41], whereas the short W–O_b and W–O_c bond lengths are slightly overestimated, by 2 and 3 per cent, in comparison with the experimental values. Concerning the long W–O_b and W–O_c bond lengths, the agreement between GGA results and experiments is quite good, whereas the LDA underestimates the experimental values by 3 and 5 per cent, respectively. The W–O bond lengths in the cubic phase (1.908 Å in the LDA and 1.935 Å in the GGA) correspond approximately to the mean length of the W–O_a bonds in the Mono RT phase.

3.2. Vacancy formation energy

The three non-equivalent oxygens of the Mono RT phase, denoted O_a, O_b and O_c, lead to the formation of the V_a, V_b and V_c neutral oxygen vacancies, respectively. The vacancy

Table 3. Formation energies E_f of neutral V_a, V_b and V_c oxygen vacancies deduced from supercell calculations at constant volume, within both the LDA and the GGA. The number of W atoms per supercell is given by n.

		Formation energy E_f (eV)			
	Supercell size n	8	**16**	32	64
LDA	V_a	4.76	**3.97**		
	V_b	4.66	**3.64**		
	V_c	4.46	**3.39**	3.07	
	Cubic	*3.43*	***2.54***		
GGA	V_a	4.12	**3.52**		3.45
	V_b	4.07	**3.06**		
	V_c	3.87	**2.87**	2.53	
	Cubic	*2.86*	***2.01***		

formation energies, E_f, obtained after relaxing the atomic positions within the LDA and GGA are reported in table 3 for the three O atoms. For both functionals, doubling the Mono RT unit cell along the W–V–W direction leads to a large decrease in E_f, comprised between 15 per cent for $E_f(V_a)$ and 25 per cent for $E_f(V_c)$. The decrease still remains significant when the unit cell is quadrupled: indeed, from the supercell with $n = 16$ to the one with $n = 32$ W atoms, the value of $E_f(V_c)$ is decreased by about 10 per cent. When doubling along the two directions perpendicular to the W–V–W direction, E_f is less affected: from the supercell with $n = 16$ to the one with $n = 64$ W atoms, the value of $E_f(V_a)$ only decreases by two per cent. This reveals the quasi-one-dimensional supercell size effect along the W–V–W direction. As shown in table 3, such a size effect is also observed in cubic supercells.

The values reported in the second column of table 3 correspond to the vacancy formation energies deduced from supercell calculations with $n = 16$ W atoms. These values are of the same order of magnitude as the ones obtained for other metal oxides using a plane-wave implementation [42]. As expected, the relaxed LDA values of E_f are larger than the GGA ones: approximately 0.5 eV larger for the three non-equivalent vacancies. This can be related to the fact that the LDA usually overestimates the binding energy in comparison with the GGA. For both functionals, the lowest value, 2.87 eV in GGA and 3.39 eV in the LDA, is obtained when removing the O_c atom, whereas the largest one, 3.52 and 3.97 eV respectively, corresponds to the formation of a V_a vacancy. The corresponding values for the formation of a V_b vacancy are intermediate: 3.06 and 3.64 eV, respectively. In the cubic phase, the value of E_f is systematically lower, independently of the choice of the functional and of the removed O atom. Nevertheless, in all cases, the total energy of the cubic supercells with a vacancy remains higher than that of the corresponding Mono RT ones.

3.3. Details of structural relaxation

When the atomic positions are unrelaxed, the hierarchy of the vacancy formation energies is reversed: thus the largest unrelaxed value is obtained for the formation of the V_c vacancy and the lowest one for the formation of the V_a vacancy. As reported in table 4, the gain in energy, ΔE, due to the structural relaxation around V_c vacancies, is very important: 2.49 eV for both functionals, whereas ΔE is lower for V_a: 1.28 and 1.53 eV within the GGA and LDA, respectively.

The detailed analysis of the structural relaxation reveals that its effect is largely one-dimensional along the W–V–W direction. Figure 2 shows such a relaxation along a W–O_c–W

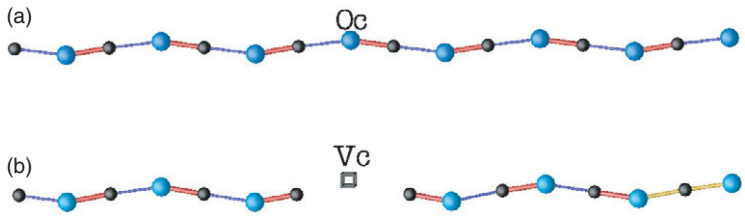

Figure 2. (a) Representation of the alternation of short (thin (blue) segments) and long (thick (red) segments) W–O bonds along the **c** crystallographic axis in WO_3 Mono RT without vacancy. (b) Modification of this alternation due to the formation of a V_c vacancy. The frustrated bonds at the edge of the cell are represented by medium (yellow) segments. W and O atoms are respectively represented by small (black) and large (blue) spheres. This last structure was obtained from a supercell GGA calculation with $n = 32$ W atoms.

Table 4. Relaxed and unrelaxed values of the formation energy E_f of the V_a, V_b and V_c oxygen vacancies. The values obtained in the cubic phase are also reported. All results are obtained at constant volume from supercell calculations with $n = 16$ W atoms, within the LDA and the GGA. The relaxation of the atomic positions leads to the gain in energy ΔE.

		Formation energy E_f (eV)		
	Vacancy	**Relaxed**	Unrelaxed	ΔE
LDA	V_a	3.97	**5.50**	*1.53*
	V_b	3.64	**5.69**	*2.05*
	V_c	3.39	**5.88**	*2.49*
	Cubic	2.54	**4.58**	*2.04*
GGA	V_a	3.52	**4.80**	*1.28*
	V_b	3.06	**5.18**	*2.12*
	V_c	2.87	**5.36**	*2.49*
	Cubic	2.01	**4.09**	*2.08*

chain. In comparison with the bulk (figure 2(a)), the number of short W–O distances remains constant along the chain with V_c (figure 2(b)). Thus, the main aspect of the structural relaxation consists in the inversion of the order of the alternation of short and long W–O distances on both sides of the vacancy. This corresponds to the conversion of a long distance into a short one. The structural relaxation is quite similar around the V_b vacancies but its amplitude is less important. Along the **a** axis, such an alternation does not really exist; hence, the structural relaxation around the V_a vacancies is weaker. In addition, the bonds at the cell boundary—represented by yellow segments in figure 2(b)—are frustrated, as their medium lengths reveal. Indeed, the short–long pattern cannot be continued across the boundary if a vacancy is present: the phase does not match there. When increasing the supercell size, the distance between two vacancies along the W–V–W direction increases, but the default resulting of the frustration is not removed.

As suggested by the one-dimensional supercell size effect on the formation energy of vacancies, the atoms belonging to the planes perpendicular to the W–V–W direction are less affected. Figure 3(a) shows the relaxed structure limited to the ten neighbouring atoms of a V_c vacancy. The displacement of the atoms located on the left side of the vacancy consists mainly in the translation along the chain. Concerning the atoms located on the right side, the displacement of the W atom along the chain leads to the conversion of a long W–O_c bond

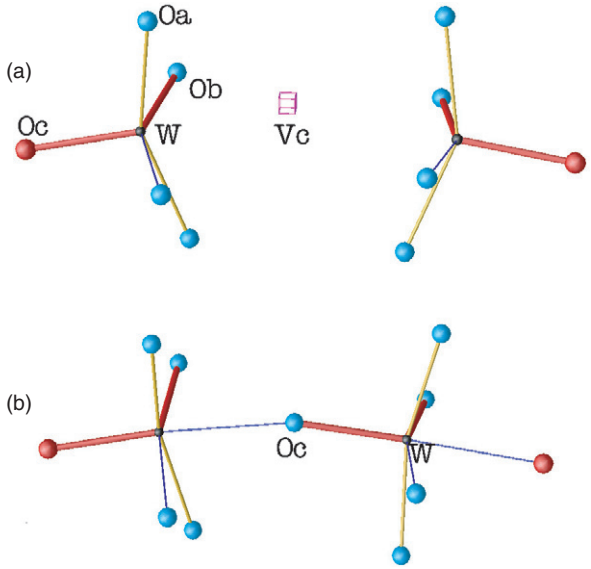

Figure 3. (a) Relaxed structure limited to the nearest neighbours of the vacancy. (b) Location of the corresponding atoms before removing the central O_c atom.

(figure 3(b)) into a short one (figure 3(a)). Thus, the left and right W–O_c bond lengths are respectively 1.77 and 1.78 Å after the structural relaxation around the vacancy, instead of 1.79 and 2.18 Å in the bulk. The motion of O_a and O_b atoms consists in a slight displacement in the direction contrary to the motion of W atoms. Consequently, the mean O_c–W–O_a and O_c–W–O_b angles around the left W atom increase from 97° to 103° and around the right W atom from 83° to 102°. The mean value of the O_a–W–O_b angles remains the same: approximately 90°. Then, the structural relaxation around V_c results in the conversion of two nearest neighbouring distorted octahedrons of the vacancy into two square-base pyramids. The structural relaxation around the V_a and V_b vacancies is similar, but its amplitude is less important.

3.4. Electronic band structure

The calculated density of electronic states (DOS) and the projected density of states (PDOS) on the valence states of O (2s, 2p) and W (6s, 5d) atoms are displayed in figure 4. Reference energy, 0 eV, corresponds to the Fermi level. For both functionals, the calculated band gap, approximately 1 eV, is largely underestimated in comparison with the experimental values of 2.62 eV [43] or 2.7 eV [44], as expected within DFT–LDA (or GGA) calculations. More advanced treatments, too time consuming for such large systems, showed that, in first approximation, the correction to the LDA consists in a rigid translation of the unoccupied bands toward higher energies, without significant changes in the occupied bands. The PDOS shows that the 2s states of oxygen atoms are located about 10 eV under the bottom of the valence band (VB). The small bandwidth, approximately 2 eV, results from a weak hybridization with the tungsten valence states. The large bandwidth of the VB, approximately 7 eV, is due to a strong hybridization between 2p valence states of oxygen and 5d valence states of tungsten. This reveals the strong covalent character of the W–O bonds.

As shown in figure 5(a), the formation of V_c induces a global shift of the band structure towards low energies, leading to the filling of the bottom of the conduction band (CB). As

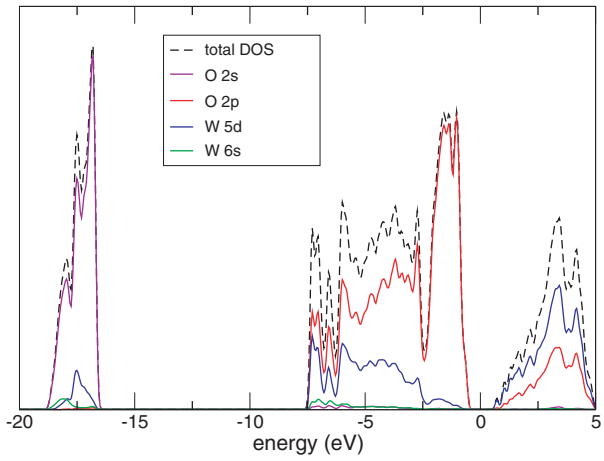

Figure 4. Total density of states (DOS) obtained by a GGA calculation in WO_3 Mono RT (dashed line). Projected density of states (PDOS) on the atomic valence states: 2s (purple line) and 2p (red line) of O, and 6s (green line) and 5d (blue line) of W.

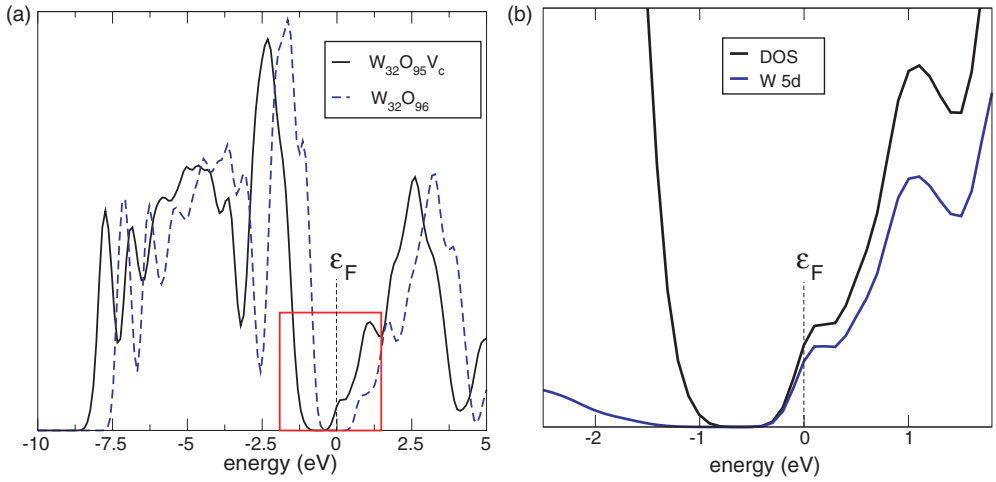

Figure 5. (a) Density of electronic states (DOS) obtained from GGA calculations in supercells containing 32 W atoms with a V_c vacancy (solid line) and in the pure phase (dashed line). (b) Enlargement centred on the bottom of the conduction band: total DOS (top line) and the 5d states of the W atoms. The reference energy (0 eV) corresponds to the Fermi level (ϵ_F).

revealed by the enlargement of the projected DOS (figure 5(b)), the new occupied electronic states involve mainly the 5d valence states of W atoms. These states could correspond to discrete levels localized in the band gap but they are not exhibited within the framework of GGA calculations, because of the underestimate of the gap. Consequently, they merge with empty states in the bottom of the conduction band. Nevertheless, our GGA calculations are qualitatively in agreement with the increase of the conductivity resulting from the formation of oxygen vacancies [21]. Moreover, they can be related to photoemission experiments, in which the magnitude of transitions involving 5d states is used in order to estimate the degree of oxygen deficiency of the surface [45].

Table 5. Mean Mulliken charge, q_i^V, carried by the different atoms i (i = W, O_a, O_b or O_c), closest to the vacancy V_c. The corresponding charge q_i in the bulk without vacancy is also reported. Charge variation on each type of atoms is given by $\Delta q_i = N_i \times (q_i^V - q_i)$, where N_i is the number of atoms i closest to the vacancy. Results, given in e^- ($1e^- = 1.610^{-19}$ C), are deduced from supercell GGA calculations with $n = 32$ W atoms.

Atom i	q_i^V	q_i	N_i	Δq_i
W	+1.60	+1.68	2	**−0.16**
O_c	−0.49	−0.52	2	**+0.05**
O_a, O_b	−0.62	−0.58	8	**−0.32**
O_c *removed*	*0*	*−0.51*	*1*	*+0.51*

The atomic charge is not a well-defined quantity and numerous models have been used to extract its value from the theoretical band structure. Within the Mulliken approach, the band structure is projected onto localized wavefunctions. Thus, the charge carried by an atom corresponds to the sum, over all the **k**-points and all the bands, of the weights of the functions localized on this atom up to the Fermi level. Its value strongly depends on the size of the basis set. Hence, the Mulliken charges reported in table 5 should be discussed only from a qualitative point of view. The LDA over-binding effect increases the strength of the W–O bonds. Thus, the ionic character of each W–O bond is less important than in the GGA and the resulting positive charge of W atoms is slightly more important in the GGA: $1.68e^-$ instead of $1.56e^-$ in the LDA. The detailed analysis of the Mulliken population of each valence state of W atoms reveals that its positive charge results from the reduced population of the 6s state: $0.35e^-$ in the Mono RT phase, instead of $2e^-$ in the isolated atom. The value of the negative charge carried by O atoms depends on the direction of W–O bonds. This anisotropy can be related to the alternation of short and long W–O bonds along the **b** and **c** directions which increases (decreases) the covalent (ionic) character of the W–O_b and W–O_c bonds in comparison with the W–O_a bonds.

Mulliken charge variations of the 12 nearest neighbouring atoms of the V_c vacancy are reported in table 5. For clarity, only the GGA variations are reported, the LDA ones being similar. The total charge of the cell with the vacancy is null and the initial charge carried by the removed O_c oxygen in the bulk ($-0.51e^-$) is mainly recovered on the W, O_a and O_b atoms closest to the vacancy. Indeed, the sum of the Mulliken charge variations of these two groups is $-0.48e^-$. More precisely, the negative variation in the charge of the two W atoms ($-0.16e^-$) results from the partial filling of the CB, which principally involves the 5d states of W atoms (as shown in figure 5). The negative charge variation ($-0.32e^-$) of the O_a and O_b atoms closest to the vacancy is induced by the increase in the weight of the orbitals localized on these atoms in the VB. The additional positive charge of the O_c atoms should be related to the decrease in the W–O_c distances corresponding to an increase in the covalent character of these bonds.

4. Conclusion

This study reveals that the neutral oxygen vacancies in the Mono RT phase are anisotropic and that the amount of relaxation correlates to the direction of the broken W–O bonds. There are three non-equivalent oxygen atoms according to the crystallographic direction of the two W–O bonds that they form. Along the **c** axis, short and long W–O bonds alternate. The corresponding unrelaxed value of the formation energy E_f of an oxygen vacancy along this direction is the largest one. In contrast, the lowest value is found for the oxygen vacancy oriented in the direction of the **a** crystallographic axis, along which oxygen atoms form intermediate length

W–O bonds. The difference in energy, 0.40 eV within the LDA and 0.55 eV within the GGA, should be related to the gain in binding energy resulting from the alternation of short and long W–O bonds. Along the **b** axis, due to an intermediate geometrical structure, the unrelaxed value of E_f is intermediate.

When the structure is relaxed, the energies go in reversed order. Thus, the lowest relaxed value of E_f is found for the oxygen vacancies along **c** and the highest one for the vacancies along **a**. We showed that this inversion is related to a strong quasi-one-dimensional structural relaxation along the **c** axis inducing an inversion of the alternation of short and long W–O distances on both sides of the vacancy. Consequently, the number of short W–O bonds remains the same. Due to the lack of significant alternation of short and long W–O bonds along the **a** axis, the structural relaxation is less important and the resulting gain in energy is approximately two times lower.

The vacancy formation induces a filling of the bottom of the conduction band involving mainly the 5d electronic states of the W atoms. This leads to an increase of the electrical conductivity of WO_3, as observed in experiments [21]. Mulliken charge analysis showed that the initial charge of the removed oxygen remains beside the nearest neighbouring atoms of the vacancy: on the two nearest W atoms because of the partial filling of the 5d states of the conduction band; and on the eight nearest O atoms because of the deformation of the valence band inducing an increase in the weight of the 2p states of these atoms. Thus the vacancy formation induces the presence of an additional localized charge. Assuming a similar electronic redistribution at the surfaces, this should lead to the formation of local electron-donor adsorption sites, which is coherent with ozone detection.

Acknowledgments

The authors thank J M Debierre and C H Mignard for fruitful discussions and for reviewing the English. Calculations were supported by the 'Centre Informatique National de l'Enseignement Supérieur' (CINES-France).

References

[1] Wriedt H A 1989 *Bull. Alloy Phase Diag.* **10** 368
[2] Davazoglou D and Donnadieu A 1987 *Thin Solid Films* **147** 131
[3] Maruyama T and Kanagawa T 1994 *J. Electrochem. Soc.* **141** 1021
[4] Granqvist C G 1995 *Handbook of Inorganique Electrochromic Materials* (Amsterdam: Elsevier)
[5] Bohnke O, Bohnke C, Donnadieu A and Davazoglou D 1998 *J. Appl. Electrochem.* **18** 447
[6] Yu A S, Kumagai N, Liu Z L and Lee J Y 1998 *J. Solid State Electrochem.* **2** 394
[7] Butler M A, Nasby R D and Quinn R K 1976 *Solid State Commun.* **19** 1011
[8] Akiyama M, Zhang Z, Tamaki J, Miura N and Yamazoe N 1993 *Sensors Actuators* B **13/14** 619
[9] Sberveglieri G, Depero L, Groppelli S and Nelli P 1995 *Sensors Actuators* B **26/27** 89
[10] Kim T S, Kim Y B, Loo K S, Sung G S and Jung H J 2000 *Sensors Actuators* B **62** 102
[11] Lee D-S, Lim J-W, Lee S-M, Huh J-S and Lee D-D 2000 *Sensors Actuators* B **64** 31
[12] Fruhberger B, Stirling N, Grillo F G, Ma S, Ruthven D, Lad R J and Frederick B G 2001 *Sensors Actuators* B **76** 226
[13] Yu-De W, Zhan-Xian C, Yan-Feng L, Zhen-Lai Z and Xing-Hui W 2001 *Solid State Electron.* **45** 639
[14] Kawasaki H, Namba J, Iwatsuji K, Suda Y, Wada K, Ebihara K and Ohshima T 2002 *Appl. Surf. Sci.* **197/198** 547
[15] Llobet E, Molas G, Molinás P, Calderer J, Vilanova X, Brezmes J, Sueiras J E and Correig X 2000 *J. Electrochem. Soc.* **147** 776
[16] Wang X, Miura N and Yamazoe N 2000 *Sensors Actuators* B **66** 74
[17] Cantalini C, Wlodarski W, Li Y, Passacantando M, Santucci S, Comini E, Faglia G and Sberveglieri G 2000 *Sensors Actuators* B **64** 182
[18] Qu W and Wlodarski W 2000 *Sensors Actuators* B **64** 42

[19] Williams D E, Aliwell S R, Pratt K F E, Caruana D J, Jones R L, Cox R A, Hansford G M and Halsall J 2002 *Meas. Sci. Technol.* **13** 923
[20] Gillet M, Lemire C, Gillet E and Aguir K 2003 *Surf. Sci.* **532–535** 519
[21] Guérin J, Aguir K, Bendahan M and Lambert-Mauriat C 2005 *Sensors Actuators* B **104** 289
[22] Hjelm A, Granqvist C G and Wills J M 1996 *Phys. Rev.* B **54** 2436
[23] Christensen N E and Mackintosh A R 1987 *Phys. Rev.* B **35** 8246
[24] de Wijs G A, de Boer P K, de Groot R A and Kresse G 1999 *Phys. Rev.* B **59** 2684
[25] Walkingshaw A D, Spaldin N A and Artacho E 2004 *Phys. Rev.* B **70** 165110
[26] de Wijs G A and de Groot R A 1999 *Phys. Rev.* B **60** 16463
[27] Karazhanov S Zh, Zhang Y, Mascarenhas A, Deb S and Wang L-W 2003 *Solid State Ion.* **165** 43
[28] Ordejón P, Artacho E and Soler J M 1996 *Phys. Rev.* B **53** R10441
[29] Soler J M, Artacho E, Gale J D, Garcia A, Junquera J, Ordejón P and Sánchez-Portal D 2002 *J. Phys.: Condens. Matter* **14** 2745
[30] Philipsen P H T and Baerends E J 1996 *Phys. Rev.* B **54** 5326
[31] DalCorso A, Pasquarello A, Baldereschi A and Car R 1996 *Phys. Rev.* B **53** 1180
[32] Filippi C, Singh D J and Umrigar C J 1994 *Phys. Rev.* B **50** 14947
[33] Hohenberg P and Kohn W 1964 *Phys. Rev.* **136** B864
[34] Perdew J P, Burke K and Ernzerhof M 1996 *Phys. Rev. Lett.* **77** 3865
[35] Troullier N and Martins J L 1991 *Phys. Rev.* B **43** 1993
[36] Sankey O F and Niklewski D J 1989 *Phys. Rev.* B **40** 3979
[37] Kehl W L, Hay R G and Wahl D 1952 *J. Appl. Phys.* **23** 212
[38] Loopstra B O and Boldrini P 1966 *Acta Crystallogr.* **21** 158
[39] Salje E K H, Rehmann S, Pobell F, Morris D, Knight K S, Herrmannsdorfer T and Dove M T 1997 *J. Phys.: Condens. Matter* **9** 6563
[40] Tanasaki S 1960 *J. Phys. Soc. Japan* **15** 566
[41] Loopstra B O and Rietveld H M 1969 *Acta Crystallogr.* B **25** 1420
[42] Tanaka I, Oba F, Tatsumi K, Kunisu M, Nakano M and Adachi H 2002 *Mater. Trans. JIM* **43** 1426
[43] Miyake K, Kaneko H, Sano M and Suedomi N 1984 *J. Appl. Phys.* **55** 2747
[44] Washizu E, Yamamoto A, Abe Y, Kawamura M and Sasaki K 2003 *Solid State Ion.* **165** 175
[45] Dixon R A, Williams J J, Morris D, Rebane J, Jones F H, Egdell R G and Downes S W 1998 *Surf. Sci.* **399** 199